Retractable Loop-Gap Resonators for Electron Paramagnetic Resonance Imaging with In Situ Irradiation Capabilities

BORIS EPEL, SUBRAMANIAN V. SUNDRAMOORTHY, HOWARD J. HALPERN

Center for EPR Imaging In Vivo Physiology, Department of Radiation and Cellular Oncology, University of Chicago, MC1105, 5841 S. Maryland Avenue, Chicago, IL 60637

ABSTRACT: A retractable split-top loop-gap resonator for both continuous wave and pulse electron paramagnetic resonance imaging of small animals with open, clam shell style design to allow convenient access to the sample for in situ animal irradiation is described. The resonator can be either rigidly attached to the animal support bed or floated independently from the bed to avoid communication of the mechanical vibrations of the bed to the resonator. Multiple split-top resonators for different animal sizes were built and tested. The characteristics of split-top resonators are comparable with those of loop-gap resonators used previously. The imaging experiments that involved the sham animal irradiation between pairs of images demonstrated very good maintenance of animal position between images. © 2011 Wiley Periodicals, Inc. Concepts Magn Reson Part B (Magn Reson Engineering) 39B: 167–172, 2011

KEY WORDS: EPR; EPR imaging; in vivo imaging; resonator

INTRODUCTION

Electron paramagnetic resonance (EPR) in vivo imaging is a rapidly developing imaging technique for the noninvasive quantitative determination of the three-dimensional distribution of spin-probe concentration and spin-probe linewidth in the tissues of living animals (*1*–*3*). The imaging technique is based on acquisition of EPR signals in the presence of applied magnetic field gradients followed by filtered backprojection image reconstruction (*4*, *5*). By applying the known relationship between spin-probe linewidth and oxygen tension, the linewidth image can be converted into an image of oxygen tension. Because of the limited penetration depth of high radiofrequency (RF) radiation in tissues, the majority of in vivo EPR imaging studies are performed at low frequencies ranging from 250 MHz to 1 GHz.

To maximize the detected signals, an animal or a portion of its body is typically placed in a resonator. Different designs of resonators have been used for magnetic resonance imaging in the past including birdcages, parallel-loop and loop-gap resonators, and surface coils (*1*, *6*–*10*). In our continuous wave (CW) and electron spin echo (ESE) studies, we use reflection type loop-gap resonators (*1*, *11*, *12*) because of their high filling factor, good magnetic field conversion efficiency, simplicity, and robustness. The access to the sample in a loop-gap resonator is only restricted by the cylindrical structure of the inductor (loop) encompassing the sample. However, for some experiments, this access is crucial. Tumor X-ray irradiation is commonly used for cancer treatment. Many aspects of the interaction between radiation and live tissues are still unknown and of great interest for medicine. To study

Received 5 July 2011; accepted 8 August 2011

Correspondence to: Howard Halpern; E-mail: h-halpern@uchicago.edu

Concepts in Magnetic Resonance Part B (Magnetic Resonance Engineering), Vol. 39B(4) 167–172 (2011)

Published online in Wiley Online Library (wileyonlinelibrary.com). DOI 10.1002/cmr.b.20205

© 2011 Wiley Periodicals, Inc.

the effect of radiation, images before and after tissue irradiation have to be obtained and compared. Detailed quantitative comparison is only possible if the before and after images are registered, that is, the spatial correspondence between voxels in the two sets of images is well established. This correspondence is straightforward if the animal is not moved relative to resonator. For correct dose deposition, the irradiation procedure requires direct unobstructed access to the surface of an animal. The irradiator head is placed at exact distance above the animal part subjected to the treatment (typically few centimeters). Areas of an animal not subjected to treatment are protected using led sheets. Positioning of the irradiator and a led shielding necessitate the removal of an animal from a conventional resonator encompassing an animal and then placing it back in the resonator for further image acquisition. Another important aspect of animal imaging is the convenience of operator during animal preparation. The installation of animal with the gas mask into a resonator rigidly mounted into the magnet is rather complicated. Animal preparation aside from the magnet saves experimental time.

The structural integrity of a resonator needs to be maintained only during imaging. Thus resonators that can be assembled for imaging and then disassembled for other procedures may be used. During nonimaging procedures, the part of resonator that provides support for the animal or its body portion can be left intact to maintain the original position of the animal. The commonly used resonators reported cannot be disassembled and assembled routinely. In this work, we examine a split-top modification of a conventional loop-gap resonator that can be used for radiation and imaging experiments.

MATERIALS AND METHODS

ESE Imaging

The imaging was performed using ESE methodology (*13*). The general design of a 250-MHz pulse imager and imaging procedures used in this study are described elsewhere (*12*). We applied three-dimensional filtered backprojection (FBP) protocol with 208 projections corresponding to an 18×18 equal solid angle gradient spacing (*14*); gradient strength was $|\vec{G}| = 15$ mT/m; five logarithmically spaced delays between 630 ns and 2.4 μs were used; object field of view was 4.24 cm, resulting image dimensions were $64 \times 64 \times 64$. For artifact reduction, 53 baseline traces (an acquisition at 1.5 mT lower than resonant field) were acquired (every fourth image projection).

Animal Imaging

Fibrosarcoma (FSa) tumors were grown on the right hind calves of 6–8-week-old C3H/HeN mice (Harlan Sprague-Dawley, Indianapolis, IN). A tumor was immobilized in the resonator by a cast of vinyl polysiloxane dental impression material (GC Dental Products, Kasugai, Japan) (*15*). The spin probe used for the EPR imaging was OX063 radical methyl-tris[8-carboxy-2,2,6,6-tetrakis[2-hydroxyethyl]benzo[1,2-d:4,5-d′] bis[1,3]dithiol-4-yl]-trisodium salt from GE Healthcare (Little Chalfont, Buckinghamshire, UK). At the start of imaging, 200 μL of 70 mM OX063 solution was injected into a 25 g animal (1.4 mmol/kg body weight). A continuous infusion of the same solution with the rate of ~ 0.22 mL per hour was maintained during the imaging. Following the first image, the animal and the resonator were moved to the irradiation facility where a sham irradiation procedure was performed. After irradiation, the resonator assembly was reinstalled in the spectrometer and a booster injection of spin probe was administered to regain signal amplitude approximately equal to that observed during the "before irradiation" image. All animal procedures were performed under Institutional Animal Care and Use Committee approved protocols.

Description of the Resonator

The split-top loop-gap resonators (Fig. 1) were built from three acrylonitrile butadiene styrene (ABS) plastic segments (parts I, II, and III). ABS ensures mechanical stability of the resonator and gives no EPR signal. Assembled together segments form a circular slab of 140-mm outer diameter with a central hole that forms an inductor loop. The ratio of the inductor loop diameter and resonator depth was kept close to 1 (Table 1). The resonators of this size are used for imaging leg bourn tumors in mice and rats. This ensures optimum filling factor of the resonator and high homogeneity of alternative magnetic field, B_1. The conductive elements that have the width equal to the thickness of the resonator are created on the side of resonator parts forming the contiguous electrically conductive surfaces a-b-c-d-e on part I, a′-b′-c′-d′-e′ on part II and f-g-g′-f′, on part III. Resonance elements and coupling capacitors are formed from the segments of these surfaces. The gap is formed between the conductive surfaces b-c of part I and b′-c′ of part II. The segments I and II are mechanically attached to each other using two screws (IV) through holes (3) and are separated by a 5–10 mils polytetrafluoroethylene (PTFE) dielectric film.

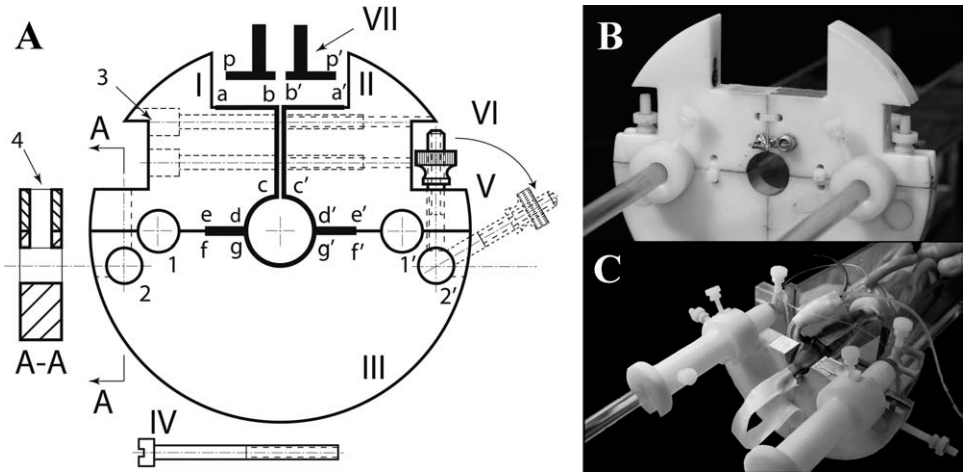

Figure 1 A: The drawing of the resonator structure. Thick lines show the conducting surfaces. The b-c and b′-c′ surfaces are separated by a dielectric spacer to form a capacitor. The c-d-g-g′-d′-c′ surfaces form a conductive loop. Surfaces e-d, f-g, and e′-d′, f′-g′ form conductive junctions. The parts I and II form the top of the resonator and are mechanically assembled using two screws (IV) through holes (3a and 3b). The top of the resonator (parts I and II) and the bottom part of the resonator (part III) are mechanically assembled using swivel bolts (V) and knurled nuts (VI). The swivel bolts rotate in the holes 2 and 2′, and enter parts I or II through a bore shown in the cut-view. The holes 1 and 1′ accommodate the parallel acrylic rods to the animal bed with ample clearance. The schematically shown coupling unit (VII) has two petals p and p′ that form capacitances with the corresponding surfaces a-b and a′-b′ of the resonator. B: The assembled resonator. The Johanson capacitor and shunt resistor across the gap are visible above the loop. The plastic clamps are used for added mechanical stability. C: Mouse leg installed into the resonator; the top part of the resonator is removed.

By selecting the thickness of the spacer, the capacitance can be varied and, consequently, the resonant frequency can be roughly adjusted (*11*). To accommodate the screws (IV), the dielectric film has corresponding holes. During normal operation of the resonator for imaging and irradiation, these two parts I and II always remain assembled. Two swivel bolts (V) with knurled nuts (VI) on both sides of the resonator part III hold the upper and the bottom halves of the resonator together and can be easily fastened and released. Additional holes in the resonator accommodate an animal bed assembly and removable plastic clamps for better electrical contact between surfaces d-e and f-g, and surfaces d′-e′ and f′-g′. In the assembled state, the surfaces c-d-g-g′-d′-c′ form an inductor loop. In this work, the conductive surfaces of the resonator were produced by application of 35 μm adhesive copper film (3M, St. Paul, MN). An alternative approach would be 12.5 μm copper and 2 μm gold depositions as it was described previously (*12*). The layer thickness was chosen to be on the order of 3–10 skin depths at 250 MHz. This thickness ensures on the one hand minimal RF radiation leakage through the walls of the resonator but on the other hand allows the conventional low frequency Zeeman modulation field used for CW measurements to enter the resonator volume.

For pulse measurements a low quality factor (Q) of the cavity is necessary to allow broadband signal detection (*9*, *12*). Low Q in our experiments is obtained by adding a shunt resistor across the gap. This resistor is installed in sockets electrically

Table 1 The Quality Factors of the Split-Top and Permanently Assembled Resonators

Resonator Dimensions	Split-Top Resonator Q	Permanently Assembled Resonator
16 mm inner diameter, 15-mm long resonator	275	330
19 mm inner diameter, 15-mm long resonator with capacitor for frequency tuning and no shunt resistor	190	220
25 mm inner diameter, 25-mm long resonator	275	300

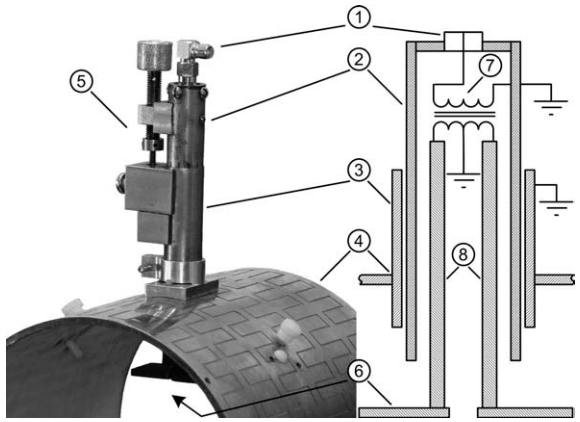

Figure 2 The photograph and schematic drawing of the coupling unit attached to the RF shield. 1: RF input; 2: inner tubing; 3: outer tubing; 4: RF shield; 5: sliding mechanism; 6: coupling plates; 7: balun transformer; and 8: brass rods.

connected to the gap and thus can be easily replaced. All RF components of our pulse system have a frequency bandwidth centered on 250 MHz. For fine tuning of the frequency of loaded resonator, we use a variable capacitor (1–30 pF Johanson 5601, Johanson Manufacturing Corporation, Boonton, NJ) across the resonator gap [see Fig. 1(B)]. Because the losses in the capacitor are proportional to its capacitance, to preserve high Q for CW measurements we adjusted the overall capacitance of resonator to utilize the lower capacitance range of variable capacitor. In resonators designed solely for CW measurements, no capacitors were installed.

The resonator RF shield is an ABS plastic tube with 12.5 μm copper and 2 μm gold deposited on its outer surface that has an outer diameter that fits the magnet gap of 145 mm with installed modulation coils. The inner diameter is equal to the outer diameter of the resonator (140 mm). The shield supports the resonator structure, the resonator coupling unit and is mounted rigidly to the magnet. For proper determination of spin-probe linewidth, the spatial uniformity of the Zeeman modulation field is of utmost importance (*16*). To improve the penetration of low frequency magnetic field inside the shield volume, the metal surface of the shield was slotted (Fig. 2, position 4). The restrictive stoppers attached to the shield ensure proper position of the resonator inside the shield. Two screws on the sides of the shield fix the resonator. The RF coupling unit is mounted on the top of the shield and penetrates the shield through the hole (Fig. 2).

We use balanced, capacitive coupling of the resonator. Unbalanced input RF power is delivered using low loss RG-7 coaxial cable and is fed into TP-101 PIN (M/A-Com, San Jose, CA) balun transformer located in the "trombone" section (Fig. 2). The mechanical design of the trombone is similar to the one described earlier (*1*). It is fabricated from two brass tubing sections. The outer tubing (3) has inner diameter of 16.1 mm, rigidly attached and electrically coupled to the RF shield. The inner tubing (2) of 15.9-mm outer diameter contains two 4-mm-diameter brass rods (8) inside, spaced by 5.2 mm center-to-center. The dimensions of rods and inner tubing were chosen appropriate for balanced 50 Ω transmission line. The electrical contact between inner and outer tubings is established by splicing a $\sim$ 2 cm section of the inner tube and springing the metal strips against the outer tubing. Two capacitor plates (p and p′ in the Fig. 1; 6 in the Fig. 2) attached to the free end of rods couple to the resonator's a-b and a′-b′ conductive surfaces. Sliding the inner tubing relative to the outer tubing allows adjustment of the distance between the plates and the resonator and thus modifies the capacitance and the resonator coupling. This provides a means for matching the resonator impedance to that of the 50 Ω RF feed line.

During an experiment, the animal body rests on an animal bed while one of the legs is extended through the resonator loop [Fig. 1(C)]. Two parallel acrylic rods that support the bed extend through holes 1 and 1′ [Fig. 1(A)] in the resonator. Rods are fastened using two sleeves whose outer diameter equals the inner diameter of the resonator service holes. The sleeve's inner diameter equals the diameter of the bed rods. Using screws, the sleeves can be fastened to the bed rods as shown in Fig. 1(B). This configuration allows the bed to attach directly to the resonator or, when the sleeves are removed, to float independently from the resonator while resting on additional support (not shown) that is mechanically decoupled from the resonator. This second operational mode is designed to reduce transmission of vibrations from a breathing animal to the resonator. Such mechanical isolation is more important for CW EPR measurements performed with the higher Q of resonator.

RESULTS AND DISCUSSION

Table 1 summarizes the resonator Q measured on the spilt-top resonators and permanently assembled resonators of equal dimensions used previously in our laboratory. One can see that the addition of two conducting joints slightly decreases the Q of the split-top resonators. Nevertheless, this Q is still considerably larger than the typical loaded Q of a resonator with a mouse of $\sim$ 100. To maintain the quality factor at

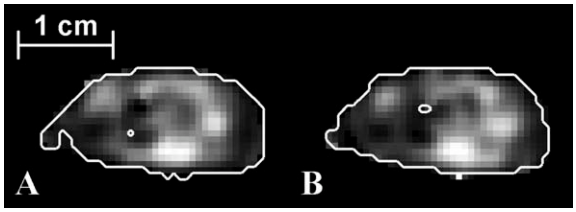

Figure 3 Saggital slices of ESE images of a mouse tumor-bearing leg before (A) and after (B) sham irradiation. The contour in (A) shows the outline (15% from the maximum) of the image (B); the contour in (B) shows the outline of the image (A). Minor differences in contours are due to slightly different spin-probe distribution in the animal. 19-mm split-top resonator, shunt resistor 700 Ω, 250 MHz, $Q = 13.4$; $|\vec{G}| = 15$ mT/m; 35 ns π/2 and π RF pulses; acquisition time 2 min.

such a good level, one has to ensure good contact between conducting surfaces. Thus the conductive surfaces of the resonator should be cleaned regularly.

We observed a considerable simplification in use of the imager equipped with the split-top resonator. Previously, the leg or body of an animal was pulled through the inductor hole of a resonator installed in the magnet, which required coordinated action of two technicians located on both sides of the magnet system. The installation of an animal into split-top resonator is performed at workbench by a single person. Gas mask, iv lines, and physiologic monitoring cables can be taped to the animal cradle, which allows a single person to relocate and install the resonator into the imager or radiation setup.

For demonstration of 19-mm split-top resonator performance, we took ESE images of the mouse leg bourn tumor separated by sham irradiation procedure (*12*). Pulse measurements require a substantial resonator bandwidth which was achieved by lowering resonator Q to 14 by installing 750 Ω shunt resistor. The representative slices of ESE images obtained before and after sham irradiation are shown in the Fig. 3. It is clear that no changes of animal position have occurred and that the images are spatially well registered. A 96% correspondence was found between the masks of the images obtained using 15% of maximum intensity threshold. No reduction of image quality in the new resonator was noticed.

CONCLUSION

The split-top loop-gap resonator is a convenient tool for low frequency EPR imaging that simplifies the operation of imager in complex experiments.

ACKNOWLEDGMENTS

The authors are grateful to Bohdan Rohowsky for remarkable precision in machining of the shield and resonators and critical look on the details of the resonator assembly design and also thank Dr. Colin Mailer and Gene Barth for preparation of this manuscript. This work is supported by NIH, grant numbers P41 EB002034 and R01 CA98575.

REFERENCES

1. Halpern HJ, Spencer DP, Vanpolen J, Bowman MK, Nelson AC, Dowey EM, et al. 1989. Imaging radiofrequency electron-spin-resonance spectrometer with high-resolution and sensitivity for in vivo measurements. Rev Sci Instrum 60:1040–1050.
2. Halpern HJ, Yu C, Peric M, Barth E, Grdina DJ, Teicher BA. 1994. Oxymetry deep in tissues with low-frequency electron-paramagnetic-resonance. Proc Natl Acad Sci USA 91:13047–13051.
3. Kuppusamy P, Chzhan M, Vij K, Shteynbuk M, Lefer DJ, Giannella E, et al. 1994. 3-Dimensional spectral spatial EPR imaging of free-radicals in the heart—a technique for imaging tissue metabolism and oxygenation. Proc Natl Acad Sci USA 91: 3388–3392.
4. Maltempo MM, Eaton SS, Eaton GR. 1987. Spectral-spatial two-dimensional EPR imaging. J Magn Reson 72:449–455.
5. Eaton GR, Eaton SS, Ohno K. 1991. EPR Imaging and In Vivo EPR. In: Eaton GR,Eaton SS,Ohno K, eds. Boca Raton FL: CRC Press.
6. Halpern HJ, Bowman MK. 1991. Low frequency EPR spectrometers: MHz range. In: Eaton GR,Eaton SS,Ohno K, eds. EPR Imaging and In Vivo EPR. Boca Raton, FL: CRC Press. pp 45–63.
7. Petryakov S, Samouilov A, Chzhan-Roytenberg M, Kesselring E, Sun ZQ, Zweier JL. 2009. Segmented surface coil resonator for in vivo EPR applications at 1.1 GHz. J Magn Reson 198:8–14.
8. Doty FD, Entzminger G, Kulkarni J, Pamarthy K, Staab JP. 2007. Radio frequency coil technology for small-animal MRI. NMR Biomed 20:304–325.
9. Devasahayam N, Subramanian S, Murugesan R, Cook JA, Afeworki M, Tschudin RG, et al. 2000. Parallel coil resonators for time-domain radiofrequency electron paramagnetic resonance imaging of biological objects. J Magn Reson 142:168–176.
10. Alecci M, Brivati JA, Placidi G, Testa L, Lurie DJ, Sotgiu A. 1998. A submicrosecond resonator and receiver system for pulsed magnetic resonance with large samples. J Magn Reson 132:162–166.
11. Froncisz W, Hyde JS. 1982. The loop-gap resonator—a new microwave lumped circuit electron-spin-resonance sample structure. J Magn Reson 47:515–521.

12. Epel B, Sundramoorthy SV, Mailer C, Halpern HJ. 2008. A versatile high speed 250-MHz pulse imager for biomedical applications. Concepts Magn Reson B Magn Reson Eng 33B:163–176.
13. Mailer C, Sundramoorthy SV, Pelizzari CA, Halpern HJ. 2006. Spin echo spectroscopic electron paramagnetic resonance imaging. Magn Reson Med 55:904–912.
14. Ahn KH, Halpern HJ. 2007. Spatially uniform sampling in 4-D EPR spectral-spatial imaging. J Magn Reson 185:152–158.
15. Haney CR, Fan X, Parasca AD, Karczmar GS, Halpern HJ, Pelizzari CA. 2008. Immobilization using dental material casts facilitates accurate serial and multimodality small animal imaging. Concepts Magn Reson B Magn Reson Eng 33B: 138–144.
16. Mailer C, Robinson BH, Williams BB, Halpern HJ. 2003. Spectral fitting: the extraction of crucial information from a spectrum and a spectral image. Magn Reson Med 49:1175–1180.